Properties of bosons in a one-dimensional bichromatic optical lattice in the regime of the pinning transition: A worm-algorithm Monte Carlo study

Asaad R. Sakhel

Department of Physics and Basic Sciences, Faculty of Engineering Technology, Al-Balqa Applied University, Amman 11134, Jordan and Abdus-Salam International Center for Theoretical Physics, Strada Costiera 11, 34151 Trieste, Italy

(Received 25 January 2016; revised manuscript received 13 June 2016; published 19 September 2016)

The sensitivity of the pinning transition (PT) as described by the sine-Gordon model of strongly interacting bosons confined in a shallow, one-dimensional, periodic optical lattice (OL), is examined against perturbations of the OL. The PT has been recently realized experimentally by Haller *et al.* [Nature (London) **466**, 597 (2010)] and is the exact opposite of the superfluid-to-Mott-insulator transition in a deep OL with weakly interacting bosons. The continuous-space worm-algorithm (WA) Monte Carlo method [Boninsegni *et al.*, Phys. Rev. E **74**, 036701 (2006)] is applied for the present examination. It is found that the WA is able to reproduce the PT, which is another manifestation of the power of continuous-space WA methods in capturing the physics of phase transitions. In order to examine the sensitivity of the PT, it is tweaked by the addition of the secondary OL. The resulting bichromatic optical lattice (BCOL) is considered with a rational ratio of the constituting wavelengths λ_1 and λ_2 in contrast to the commonly used irrational ratio. For a weak BCOL, it is chiefly demonstrated that this PT is robust against the introduction of a weaker, secondary OL. The system is explored numerically by scanning its properties in a range of the Lieb-Liniger interaction parameter γ in the regime of the PT. It is argued that there should not be much difference in the results between those due to an irrational ratio λ_1/λ_2 and those due to a rational approximation of the latter, bringing this in line with a recent statement by Boers *et al.* [Phys. Rev. A **75**, 063404 (2007)]. The correlation function, Matsubara Green's function (MGF), and the single-particle density matrix do not respond to changes in the depth of the secondary OL V_1. For a stronger BCOL, however, a response is observed because of changes in V_1. In the regime where the bosons are fermionized, the MGF reveals that hole excitations are favored over particle excitations manifesting that holes in the PT regime play an important role in the response of properties to changes in γ.

DOI: 10.1103/PhysRevA.94.033622

I. INTRODUCTION

It is known that weakly interacting bosons confined by a deep periodic one-dimensional (1D) optical lattice (OL) undergo a transition from a superfluid (SF) to a Mott insulator (MI) [1–4] when the strength of the OL is increased. The opposite situation of getting another kind of SF-to-MI transition in a shallow 1D OL occupied by strongly interacting bosons [5–7] is known as the pinning transition (PT), where the bosons are "pinned" just by subjecting them to a very weak periodic OL. Indeed, the PT has been first observed by Haller *et al.* [5], although its concept has been communicated and examined earlier [6,8], even later on in a hollow-core 1D fiber [9].

The main goal of this article is the examination of the sensitivity of this PT against perturbations. In that sense, we tweak the PT by the addition of a second disordering OL component to establish a 1D bichromatic optical lattice (BCOL), a method that has been used elsewhere [10–12]. Since the latter PT has been realized experimentally and followed later by another observation and analytical examination by Boéris *et al.* [7] and Astrakharchik *et al.* [13], it is justified to explore its stability under a perturbation of the OL. The chief result of our work is that the PT is robust against the latter perturbations.

Bóeris *et al.* [7] studied the PT in shallow 1D periodic OLs. Their quantum Monte Carlo calculations verified the predictions of the Bose-Hubbard model (BHM). They have shown, both theoretically and experimentally, that the critical points for the PT deviate from those predicted by the sine-Gordon (SG) model [6] and that they are close to the BHM. In a related work, Astrakharchik *et al.* [13] investigated an interacting 1D Bose gas in an OL using the diffusion Monte Carlo method. Their results for the PT critical points were found to agree with the discrete BHM. It has been demonstrated that the SG model for shallow lattices is inaccurate. Notwithstanding the fact that the purpose of the present work is not to check the accuracy of the SG theory, it nevertheless turns out that our critical points for the PT deviate likewise from SG theory, bringing this in line with [7,13].

Although investigations using BCOLs are quite abundant, the literature on the effects of perturbing the primary OL is lacking; nevertheless there have been a few earlier studies about this, but within a different context. For example, Edwards *et al.* [14] studied the effects of localization on the loading of a Bose-Einstein condensate into a shallow 1D BCOL. It has been found that the effects due to the addition of a secondary component disappeared as interactions got stronger. We can relate to this result since our simulations are in the strongly interacting regime and yield analogously a robustness of the PT against the latter perturbations for shallow BCOLs. According to Edwards *et al.*, the latter result is due to the fact that increased interactions yield a suppression of the long-wavelength wave-function modulations. In the case of noninteracting quantum particles, Boers *et al.* [15] explored localization properties in a 1D BCOL. It has been shown that for a shallow BCOL the sharp metal-insulator transition shown by the tight-binding model is replaced with a sequence of mobility edges.

Another goal is the examination of the properties of the bosons in the regime of this PT as measured by the

pair correlation function $g_2(r)$ and one-body density matrix (OBDM) $g_1(r)$ (with r the distance between a pair of particles), the Matsubara Green's function (MGF) $G(p=0;\tau)$, and SF fraction ρ_s/ρ. It must be emphasized that in this work the $g_2(r)$ of the homogeneous Bose gas is intentionally applied to bosons in a 1D BCOL, for mathematical convenience, to account for the density-density correlations (that are related to $g_2(r)$ [16,17]) under the effect of a BCOL. On the other hand, for inhomogeneous systems, the pair correlation function and OBDM are normalized by the spatially varying density instead of the average linear density. A key result is that for a shallow 1D OL, the above properties are not influenced by perturbations of the OL. We particularly focus on $g_2(r)$ because it is important to examine it with regards to this and other kinds of phase transitions. For example, the pair correlation function for a 1D uniform Bose gas has been used as the ratio between the photoassociation rates of Rb^{87} atoms in 1D and 3D [18]. Although we examine it only briefly, the $g_1(r)$ is also not any less important; for example, Deissler *et al.* [19] presented the first experimental analysis of $g_1(r)$, similar to ours, in a quasiperiodic optical lattice (QPOL).

Indeed, the role of a 1D OL, such as the BCOL [10,11], in conjunction with atom-atom interactions in defining the properties of confined bosons, lies at the heart of many investigations today [12,18,20–24]. So far, the BCOL has been mostly applied to introduce quasidisorder in a "common experimental route" [12]. This is usually achieved by superimposing two OL wavelengths whose ratio λ_1/λ_2 yields an irrational number [20,22,23]. However, the lattice setup with a rational number λ_1/λ_2 is not very common and deserves, therefore, an investigation, particularly due to the likelihood that there may be not much difference between the use of a rational and irrational λ_1/λ_2. For noninteracting quantum particles in a 1D BCOL, Boers *et al.* [15] stated (quoting them) "... it is not necessary to implement truly irrational numbers with mathematical (i.e., unattainable) precision; after all, on a finite lattice one can 'resolve' only a finite number of digits." In fact, real disorder can only be achieved by a speckle potential and the investigation of bosons in this kind of potential (and add to this a quasidisordered one) has been going on intensively in the past few years [11,15,19,21,23,25–52].

The bosons in the BCOL are simulated using the continuous-space worm-algorithm (WA) quantum Monte Carlo approach [53]. The WA is a powerful method giving an accurate estimate of physical observables, such as ρ_s/ρ, $g_1(r)$, $g_2(r)$, density, etc. The ρ_s/ρ is plotted as a function of the Lieb-Liniger interaction parameter γ [54] for various realizations of the BCOL. It is verified again that WA reproduces the PT accurately and that the interplay of BCOL and interactions has little effect on changing the critical interaction at which this PT occurs. The PT-critical points are close to those of Boéris *et al.* [7]. In other results, (1) the OBDM of the system displays substantial depletion of the SF as it passes through the PT; (2) the MGF shows signals for fermionization detected via the correlation function at the origin, $g_2(0)$, when the total interaction energy goes to zero, demonstrating perfect antibunching [55]; (3) the secondary OL has been found not to play a role in aiding or preventing the fermionization.

The organization of the present paper is as follows. Section II presents the method and Sec. III represents the results. Section IV discusses the issue of a rational and irrational ratio of the BCOL wavelengths and in Sec. V the paper concludes with some closing remarks. In Appendix A the WA is briefly described. In Appendixes B, C, and D, the correlation functions that are normalized by the spatially varying density are examined. In Appendix E the WA code is tested for accuracy as applied to the present system.

II. METHOD

A brief description of the WA applied to the present system is relegated to Appendix A and it is tested for accuracy in Appendix E. The simulations have been conducted on the excellent computational cluster of the Max Planck Institute for Physics of Complex Systems in Dresden, Germany. In essence, the present work has been a heavily computational project with each simulation taking about a week of CPU time to finish.

A. Optical lattice

In order to introduce disorder into the present system, the WA code [56]—originally designed for a homogeneous Bose gas—has been modified by including a BCOL potential of the form

$$V_{OL}(x) = V_0 \cos^2(\alpha\pi x) + V_1 \cos^2(\beta\pi x), \tag{1}$$

where V_0 and V_1 are the primary- and secondary-OL depths, respectively, and we always consider $V_1 < V_0$. The parameters $\alpha = 2/\lambda_1$ and $\beta = 2/\lambda_2$, with λ_1 and λ_2 the wavelengths, determine the periodicity of the BCOL and such a type of lattice was shown to realize disorder [11,29]. α and β were set to 0.4 and 1.0, respectively, for a QPOL and 0.4 and 1.39 for a quasidisordered optical lattice (QDOL).

A measure for the strength of the BCOL quasidisorder is its standard deviation δV given by

$$\delta V = \sqrt{\langle V^2\rangle - \langle V\rangle^2}, \tag{2}$$

with

$$\langle V\rangle = \frac{1}{L}\int_0^L V_{OL}(x)dx \tag{3}$$

and

$$\langle V^2\rangle = \frac{1}{L}\int_0^L V_{OL}^2(x)dx, \tag{4}$$

where L is the length of the system.

B. Interactions

The interactions between the bosons are accounted for by the exact two-particle density matrix given by (see, e.g., Feynman [57])

$$\rho(x_1-x_2) = 1 - \sqrt{\frac{\tau}{4ma_s^2}}\exp\left\{\frac{m}{4\tau}(x_1-x_2)^2 + \frac{|x_1|+|x_2|}{a_{1D}} + \frac{\tau}{ma_{1D}^2}\right\}, \tag{5}$$

where $\tau = \beta/M$ is the "time step," with $\beta = 1/(\widetilde{T}T_d)$, $\widetilde{T}$ being the temperature in units of the degeneracy temperature

T_d, $k_B = 1$ Boltzmann's constant, and $m = 0.5$ is the boson mass. Equation (5) appears in the worm-update probabilities as a multiplicative factor. The interactions are then essentially described by a δ function $g_{1D}\delta(x_1 - x_2)$, where g_{1D} is the interaction parameter.

In Astrakharchik *et al.* [58], g_{1D} is given by

$$g_{1D} = -\frac{2\hbar^2}{m a_{1D}}, \tag{6}$$

where $\hbar$ is Planck's constant and a_{1D} the scattering length. Essentially, the absolute value of g_{1D} is considered in the present calculations. From Haller *et al.* [5], the Lieb-Liniger parameter is given by

$$\gamma = m g_{1D}/(\hbar^2 n), \tag{7}$$

where $n = \langle N\rangle/L$ is the average linear density with $\langle N\rangle$ the thermodynamic average of the particle number.

C. Pair correlation function

The spatially averaged pair correlation function (SAPCF) for the 1D homogeneous Bose gas is given by

$$g_2(r) = \frac{1}{L n^2}\int_0^L dx \langle \hat\psi^\dagger(x+r)\hat\psi^\dagger(x)\hat\psi(x)\hat\psi(x+r)\rangle, \tag{8}$$

where r is the distance between any two particles along the system and $\hat\psi(x)$ [$\hat\psi^\dagger(x)$] is the field operator annihilating [creating] a boson at position x. It can account for the spatially averaged density-density correlation function [59], given by

$$n_c(r) = \frac{1}{L}\int_0^L dx \langle \hat n(x+r)\hat n(x)\rangle. \tag{9}$$

On the other hand, when $g_2(r)$ is normalized by the convolution of two spatially varying densities, $\rho(x)$ and $\rho(x+r)$, that is,

$$\rho_c(r) = \frac{1}{L}\int_0^L dx \rho(x+r)\rho(x) \tag{10}$$

instead of n^2, where $\rho(x) = \langle\hat\psi^\dagger(x)\hat\psi(x)\rangle$, one gets the SAPCF for an inhomogeneous Bose gas given by [60,61]

$$h_2(r) = \frac{\int_0^L dx \langle \hat\psi^\dagger(x+r)\hat\psi^\dagger(x)\hat\psi(x)\hat\psi(x+r)\rangle}{\int_0^L dx \rho(x+r)\rho(x)}. \tag{11}$$

The examination of $h_2(r)$ is relegated to Appendix B .

D. One-body density matrix

The spatially averaged one-body density matrix (SA-OBDM) for the 1D homogeneous Bose gas is defined as

$$g_1(r) = \frac{1}{Ln}\int_0^L dx \langle \hat\psi^\dagger(x+r)\hat\psi(x)\rangle, \tag{12}$$

and again for the inhomogeneous case [61]

$$h_1(r) = \frac{\int_0^L dx \langle \hat\psi^\dagger(x+r)\hat\psi(x)\rangle}{\rho_{c,\frac{1}{2}}(r)}, \tag{13}$$

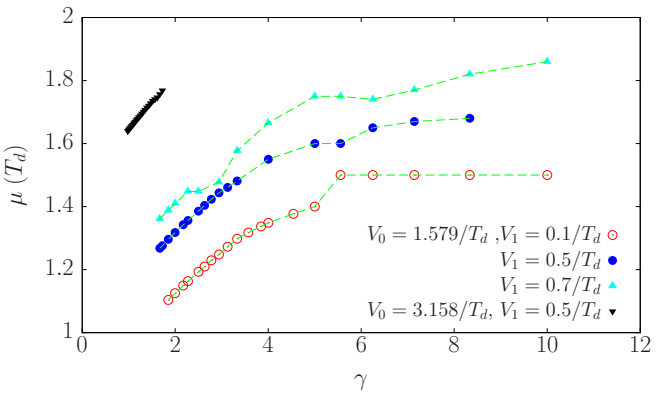

FIG. 1. Calibrated chemical potential μ as a function of γ for the commensurate filling of a number of BCOLs with $\alpha = 0.4$ and $\beta = 1.0$ at $N = 200 \pm \delta$ particles, where δ is a small error. The figure displays the case for $V_0 = 1.579/T_d$ and $V_1 = 0.1/T_d$ (open circles); $0.5/T_d$ (solid circles); $0.7/T_d$ (solid up triangles); and then the case for $V_0 = 3.158/T_d$ and $V_1 = 0.5/T_d$ (solid down triangles). μ is in units of T_d and γ is unitless.

where

$$\rho_{c,\frac{1}{2}}(r) = \frac{1}{L}\int_0^L dx \sqrt{\rho(x+r)\rho(x)}. \tag{14}$$

The examination of $h_1(r)$ is also relegated to Appendix C. $\rho_c(r)$ and $\rho_{c,\frac{1}{2}}(r)$ are from now on referred to as the "convoluted densities."

E. Chemical potential and interactions

The total number of particles $\langle N\rangle$ for each γ was fixed to 200 by a careful tuning of the chemical potential μ from a calibration curve, i.e., a plot of $\langle N\rangle$ versus μ for each interaction strength γ. That is, after a long WA simulation time, the number of particles stabilizes at $\langle N\rangle = 200$ for all systems. The error bars δ in $N = \langle N\rangle \pm \delta$ are within ± 1 (in fact $\ll 0.1$) and this error is unavoidable as one is dealing with a continuous-space Monte Carlo simulation. Figure 1 displays a plot of the calibrated μ versus γ for a number of BCOL realizations. The μ rises in general with γ until it begins to stabilize in the strongly interacting PT regime.

F. Units and parameters

The degeneracy temperature is given by $T_d = 2\pi\hbar^2 n^2/m$ and the photon recoil energy by $E_R = h^2/(2m\lambda^2)$; their ratio is always $T_d/E_R = 4/\pi$. From Eqs. (6) and (7) one gets $\gamma = -2/(a_{1D}n)$. Here λ is the wavelength of the laser beams creating the OL where $\lambda = 2d$ is twice the primary lattice period d [$= 1/\alpha$; cf. Eq. (1)] and $n = 2/\lambda$ is the average linear density. Technically speaking, it should be emphasized that T_d is set by an initial density parameter n_0 that is input into the WA program and used to initialize the size of the system. Since the present simulations are in the grand-canonical ensemble, we carefully calibrated μ as in Sec. II E so that the final density of the system n always ends up the same as n_0 at the end of the WA simulation. (Both $\langle N\rangle$, L, and therefore T_d are then the same for all systems.) An OL depth like, e.g., 1.0 in units of E_R corresponds to $V_0 = 1.0E_R/T_d = 1.0 \times \pi/4 = 0.785$ in

units of T_d. Now in the WA code $m = 0.5$, $\hbar = 1$, λ/L=0.01, and $n\lambda = 2.0$, and therefore $T_d = 4\pi n^2 = 0.64\pi$ and $E_R = 4\pi^2\hbar^2/(2m\lambda^2) = 0.16\pi^2$. The temperature is set to $\widetilde{T} = T/T_d = 0.001$ to allow a significant value of ρ_s/ρ.

The length of the system is such that $2L/\lambda = 200$ lattice sites and is at almost perfect commensurate filling. For purposes of comparison, the value of the wavelength is the same as that used by Haller *et al.* [5]; namely, $\lambda = 1064.5$ nm and the values for the OL depth V_0 are of the same order of magnitude as in Haller *et al.* [5], Gordillo *et al.* [12], and Boéris *et al.* [7]. In [12], the wavelength of the laser beams generating the OL was $\lambda = 830$ nm and considering that the 3D scattering length of Rb^{87} is almost $100a_0$, the 1D Lieb-Liniger interaction parameter becomes $\gamma = 1.770$. The values of γ used in the present work are in general, larger than in Ref. [12] as they extend into the strongly interacting PT regime.

III. RESULTS

A. Pinning transition

An important result of this work is that the WA is able to reproduce the PT [5,7] in a 1D shallow periodic OL. It is found that the latter PT is robust against perturbations arising from the addition of a weaker secondary OL. The critical value γ_c at which the PT occurs in a BCOL (1) remains exactly the same as compared to a periodic OL with the same V_0, unaffected by the latter perturbations. This is the chief result of this paper and is demonstrated by the behavior of ρ_s/ρ as a function of γ for a Bose gas in various realizations of a 1D BCOL (1). Figure 2 demonstrates this finding for two values of the primary depth $V_0^{(a)}$ and $V_0^{(b)}$ and different strengths of the associated secondary OL, $V_1^{(a)}$ and $V_1^{(b)}$, respectively. Here ρ_s/ρ displays a steep decline towards the critical γ_c beyond which it remains zero deep into the PT regime $\gamma \gg \gamma_c$. The value of γ_c, indicated by a vertical dashed line, is obtained by fitting a function of the form $f(\gamma) = A(\gamma_c - \gamma)^s$ to the data of ρ_s/ρ in a narrow range of γ, where ρ_s/ρ comes close to zero. Here A, γ_c, and s are fitting parameters. We return to this issue in a future publication, where a comparison between WA numerical and experimental results is required in order to explore the validity of the SG theory [7,13] at higher temperatures. The addition of a secondary OL does not alter the behavior of ρ_s/ρ from the one observed for $V_1^{(a,b,c)} = 0$, the purely periodic OL. For $V_0^{(c)} = 1.579/T_d$, the behavior of ρ_s/ρ in frame (b) with $\beta/\alpha = 3.475$ is exactly the same as in frame (a) with $\beta/\alpha = 2.5$ and the same $V_0^{(a)} = 1.579/T_d$. This is a rather peculiar result showing that an increased quasidisorder in a shallow BCOL does not alter the behavior of ρ_s/ρ. From Fig. 2, we obtain $1/\gamma_c = 0.2944 \pm 0.008$ for $V_0 = 1.579/T_d$ $(= 1E_R)$ and 0.5794 ± 0.017 for $3.158/T_d$ $(= 2E_R)$. They are close to the ones obtained by Boéris *et al.* [7], being $1/\gamma_c = 0.3638 \pm 0.036$ and 0.5072 ± 0.031 for $V_0 = 1.04$ and $2.05E_R$, respectively. (The latter numbers of Boéris *et al.* have been extracted from their Fig. 3 using a special tool.) In that sense, the critical points given by the SG model for $V_0 = 1$ and $2E_R$, being $1/\gamma_c = 0.4515$ and 0.7122, respectively, clearly differ from our critical points, bringing this in line with Refs. [7,13]. This is again a striking demonstration of the fact that the WA is a powerful method enabling an accurate simulation of the behavior of lattice bosons in continuous space.

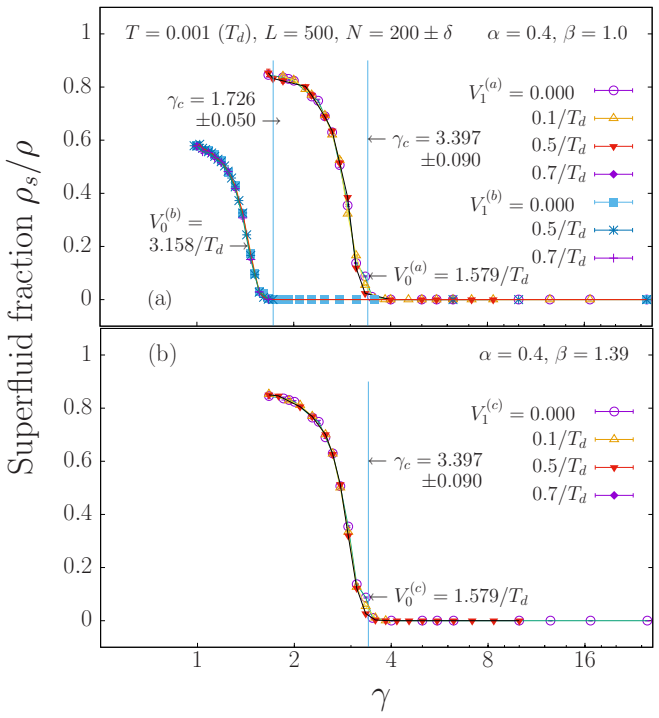

FIG. 2. Worm-algorithm superfluid fraction ρ_s/ρ versus the Lieb-Liniger parameter γ for an interacting Bose gas in several realizations of the BCOL. The figure demonstrates primarily the WA numerical reproduction of the pinning transition observed experimentally in Ref. [5]. The temperature of the system is $\widetilde{T} = 0.001$, its length L is such that $2L/\lambda = 200$, and the thermodynamic average particle number $\langle N \rangle$ is 200 with a small error δ that is within the range ± 1 ($|\delta| \ll 0.1$). Two primary-OL depths $V_0^{(a)} = 1.579/T_d$ and $V_0^{(b)} = 3.158/T_d$ are considered with different associated depths $V_1^{(a)}$ and $V_1^{(b)}$ of the superimposed secondary OLs, respectively. Each of the primary OLs has exactly 200 sites with an occupancy of one particle per site in the PT regime. Panel (a) is for a QPOL with $\alpha = 0.4$ and $\beta = 1.0$. Open circles, $V_1^{(a)} = 0.000$ (purely periodic OL); open up triangles, $0.1/T_d$; solid down triangles, $0.5/T_d$; and solid diamonds, $0.7/T_d$. Solid squares, $V_1^{(b)} = 0.000$; stars, $0.5/T_d$; and crosses, $0.7/T_d$. Panel (b) is for a quasidisordered OL with $V_0^{(c)} = 1.579/T_d$, the same α, but a different $\beta = 1.39$. The labels for $V_1^{(c)}$ are the same as for $V_1^{(a)}$. The vertical dashed lines show the PT points $\gamma_c = 3.397 \pm 0.090$ for $V_0^{(a)} = V_0^{(c)} = 1.579/T_d$, and 1.726 ± 0.050 for $V_0^{(b)} = 3.158/T_d$ which are close to the ones found by Boéris *et al.* [7]. V_0, V_1, and $\widetilde{T}$ are in units of T_d and γ is unitless.

The robustness of ρ_s/ρ against the secondary-OL perturbations arises because the particles always seek the lowest energy states of the BCOL, i.e., those of the primary OLs. Further, in the strongly interacting regime $\gamma > 1$, the interactions override the effects introduced by V_1 as the behavior of bosons is chiefly dictated by the commensurate filling of the primary OL. This finding is brought in line with that of Boéris *et al.* [7], who argued that in the limit of a shallow periodic potential the optical depth becomes subrelevant when the Mott transition is controlled only by interactions.

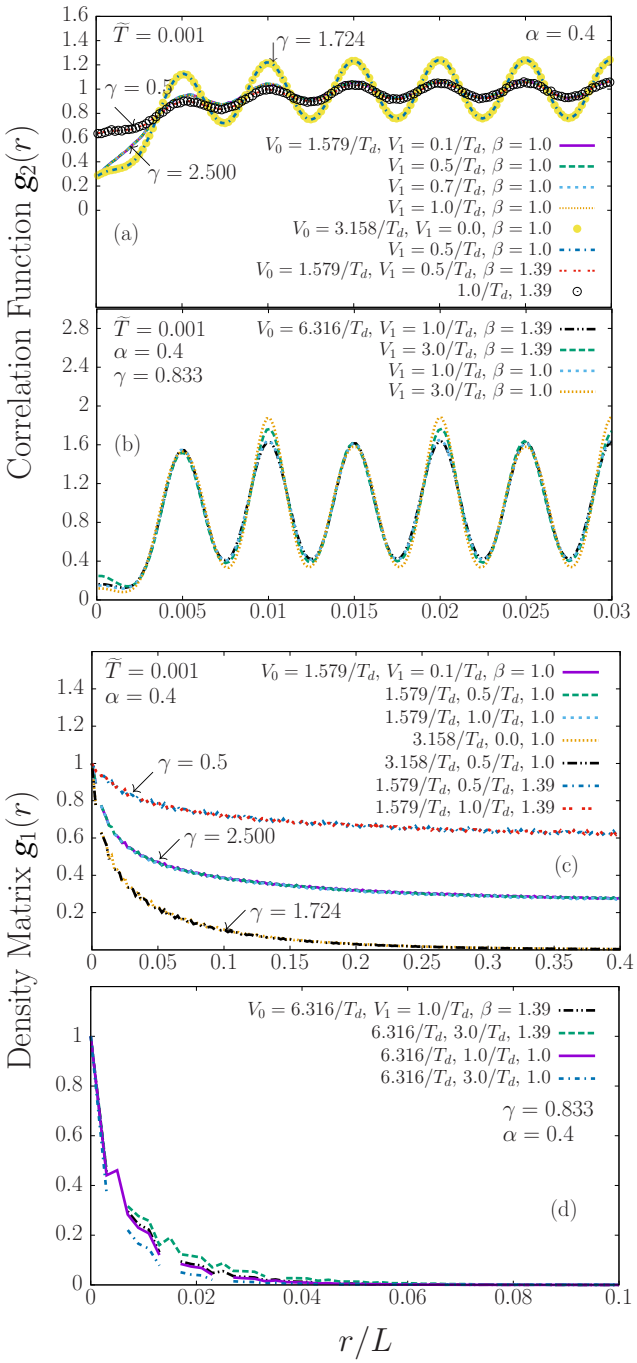

FIG. 3. Effect of secondary optical lattice on the spatially averaged correlation function $g_2(r)$ [Eq. (8)] and the spatially averaged density matrix $g_1(r)$ [Eq. (12)] of the systems in Fig. 2. Here r is the distance between any pair of particles along the lattice and all frames share the same x-axis label. Panel (a) shows $g_2(r)$ for $\alpha = 0.4$ at different interaction strengths and for various BCOL realizations. For $\gamma = 2.500$, $V_0 = 1.579/T_d$, and $\beta = 1$, the figure displays the cases for $V_1 = 0.1/T_d$ (solid line); $0.5/T_d$ (long-dashed line); $0.7/T_d$ (dotted line); $1.0/T_d$ (fine-dotted line). (It is difficult to plot these lines so that all symbols can be distinguished from each other because they are exactly overlapping. The same applies to the rest of the plots.) For $\gamma = 1.724$, $V_0 = 3.158/T_d$, and the same β, the figure shows the cases for $V_1 = 0.0$ (solid circles) and $0.5/T_d$ (dash-dotted line). The last set of data is for $\gamma = 0.5$, $V_0 = 1.579/T_d$, but with $\beta = 1.39$ and $V_1 = 0.5/T_d$ (double-dotted line) and $1.0/T_d$ (open circles). Panel (b) is as in (a), except for $V_0 = 6.316/T_d$, $\gamma = 0.833$, and $V_1 = 1.0/T_d$ with $\beta = 1.39$ (dash-double-dotted line), $3.0/T_d$ with 1.39 (thick-dashed line), $1.0/T_d$ with 1.0 (dotted line), and $3.0/T_d$ with 1.0 (fine-dotted line). Going over to $g_1(r)$, panel (c) displays it for $\gamma = 2.500$, $V_0 = 1.579/T_d$, and $V_1 = 0.1/T_d$ with $\beta = 1.0$ (solid line), $0.5/T_d$ and 1.0 (thick-dashed line), and $1.0/T_d$ and 1.0 (dotted line). The following set of data is for $\gamma = 1.724$, $V_0 = 3.158/T_d$ and $V_1 = 0.000$ with $\beta = 1.0$ (fine-dotted line), and $0.5/T_d$ with $\beta = 1.0$ (dash-double-dotted line). Next comes $V_0 = 1.579/T_d$, $\gamma = 0.5$, and $V_1 = 0.5/T_d$, with $\beta = 1.39$ (dash-dotted line) and $1.0/T_d$ and 1.39 (double-dotted line). Finally, panel (d) is as in (c), except for $V_0 = 6.316/T_d$, $\gamma = 0.833$, and $V_1 = 1.0/T_d$ with $\beta = 1.39$ (dash-double-dotted line), $3.0/T_d$ and 1.39 (dashed line), $1.0/T_d$ and 1.0 (solid line), and $3.0/T_d$ and 1.0 (dash-dotted line). The r is in units of L, $\widetilde{T}$ is in units of T_d, and γ is unitless.

B. Effect of secondary lattice

Figure 3 shows the influence of V_1 on the spatial behavior of $g_1(r)$ and $g_2(r)$, particularly the amplitudes of the $g_2(r)$ oscillations, for various realizations of the BCOL. A significant feature is that $g_2(r)$ reveals a spatial oscillatory structure whose origin can be traced back to the primary OL. On the other hand, $g_1(r)$ in panel (c) displays a structure similar to that of $g_1(r)$ of the 1D homogeneous Bose gas in Fig. 10 of Appendix E without any spatial oscillations.

As V_0 increases, so do the oscillatory amplitudes of $g_2(r)$ in panel (b) displaying its deep connection to the OL. An enhanced spatial decay rate of $g_1(r)$ at larger V_0 in panel (c) indicates a reduction of the SF fraction. The spatial frequency of the $g_2(r)$ oscillations changes neither with V_0 nor with V_1 and is largely governed by the lattice parameter of the primary OL. When V_0 and V_1 are small, e.g., $\sim 1.5/T_d$ in panels (a) and (c), a change of V_1 does not alter the spatial behavior. Remarkably, the secondary OL is practically not "seen" by the bosons in this case. The $g_1(r)$ and $g_2(r)$ for bosons in a QPOL ($\beta = 1.0$) do not differ from those in a QDOL ($\beta = 1.39$). However, when V_0 is increased to larger values $\sim 6/T_d$ as in panels (b) and (d), a change in the band structure of the BCOL via V_1 and β begins to assert itself in $g_2(r)$ and $g_1(r)$. Further, at larger $V_0 = 6.316/T_d$, the change in the oscillatory amplitude of $g_2(r)$ with V_1 is more pronounced for a QPOL than for a QDOL, indicating that an increased disorder does not necessary yield a stronger response to V_1. The same argument can be applied to $g_1(r)$ in panel (d). The secondary OL begins to influence the properties only in conjunction with a larger V_0 at which the BCOL begins to compete with the boson-boson interactions. Indeed, the difference in β/α introduces a difference between the band structures of the QPOL and the QDOL and therefore the corresponding $g_2(r)$.

C. Effect of interactions on the correlations

Figure 4 demonstrates the effect of interactions on $g_2(r)$ for all realizations of the BCOL. The qualitative pattern of these oscillations hardly changes with γ (and V_1), even on going through the PT. Quantitatively, however, the amplitude of these oscillations rises, in general, in response to an increase of γ (and V_0). [Compare frame (c) with both (a) and (b).] The latter manifests an increase in the interplay between the interactions

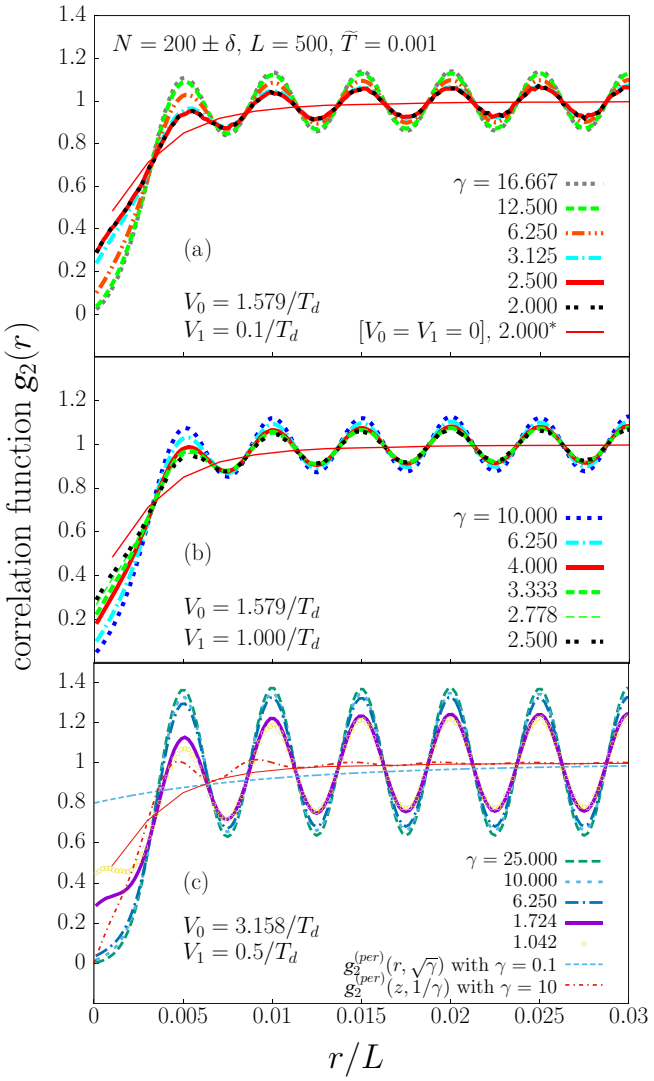

FIG. 4. Worm-algorithm pair correlation function $g_2(r)$ [Eq. (8)] at various interactions γ for the systems of Fig. 2(a) and three realizations of the BCOL with $\alpha = 0.4$ and $\beta = 1.0$. Panel (a) is for the BCOL of primary depth $V_0 = 1.579/T_d$ and a secondary depth $V_1 = 0.1/T_d$ at $\gamma = 16.667$ (dotted line), 12.500 (dashed line), 6.250 (dash-triple-dotted line), 3.125 (dash-dotted line), 2.500 (thick solid line), and 2.000 (double-dotted line). For additional comparison, the thin solid line is exceptionally displayed for a homogeneous Bose gas without an OL ($V_0 = V_1 = 0$) at $\gamma = 2.000$ and the same parameters as in Fig. 2(a). It is also displayed in panels (b) and (c). Panel (b) is as in (a); but for $V_1 = 1.0/T_d$ and $\gamma = 10.000$ (dotted line), 6.250 (dash-dotted line), 4.000 (thick-solid line), 3.333 (thick-dashed line), 2.778 (thin-dashed line), 2.500 (double-dotted line). Panel (c) is for $V_0 = 3.158/T_d$, $V_1 = 0.5/T_d$, and $\gamma = 25.000$ (dashed line), 10.000 (dotted line), 6.250 (dash-dotted line), 1.724 (thick solid line), 1.042 (circles). The thin-dashed and thin-dashed-dotted lines show the analytic results $g_2^{(per)}(z, 1/\gamma)$, with $z = n\pi r$ [Eq. (17)] at $\gamma = 10$ and $g_2^{(per)}(r, \sqrt{\gamma})$ [Eq. (18)] at $\gamma = 0.1$ from Ref. [55]. The plot for these functions was generated by *Mathematica*. There is almost perfect commensurate filling with $N = 200 \pm \delta$ particles, where δ is a small error in the range ± 1 ($|\delta| \ll 0.1$). V_0, V_1, and $\widetilde{T}$ are in units of T_d, and γ is unitless.

and the BCOL that in turn enhances the boson-boson [i.e., density-density $n_c(r)$] correlations. It must be emphasized that the rise in the amplitude of $g_2(r)$ oscillations is particularly significant beyond γ_c reaching deep into the PT regime where the bosons are pinned. This is therefore indicative of a Mott insulator (MI) state which is not inert. An examination of the MGF $G(p = 0, \tau)$ in Sec. III G and by making connections to $g_2(r)$, it is inferred that holes, arising from particle-hole (p-h) excitations, play an important role in the enhancement of $g_2(r)$.

On the one hand, the response of $g_2(r)$ to γ can be further clarified by other arguments. First, it is known that $g_2(r)$ [Eq. (8)] describes the probability of finding two particles at a separation r. Hence, as the bosons become more localized with increasing γ, the probability—i.e., the amplitude of $g_2(r)$ oscillations—rises. Second, when the interactions are large, higher harmonics in the density operator $\widetilde{\rho}(x)$ from Ref. [8] become excited, playing a role in intensifying $g_2(r)$. Here $\psi(x) = \sqrt{\widetilde{\rho}(x)}\exp[i\varphi(x)]$ is a field operator with $\varphi(x)$ a phase and [8,20]

$$\widetilde{\rho}(x) = \left\{ n^2 + \frac{1}{\pi^2}[\nabla\phi(x)]^2 + n^2 \sum_{p>1} \cos[2\pi n x - 2p\phi(x)] \right\}^{1/2}, \tag{15}$$

where $\phi(x)$ is a boson-field operator and n the average density. On the other hand, the rise in the amplitude with V_0 can be related to the amplitude of the Wannier state in each OL well. For sufficiently deep OLs, the Wannier state can be approximated by a harmonic oscillator ground state [15],

$$W(x) = \frac{k^{1/2}}{\pi^{1/4}} \left(\frac{V_0}{E_r}\right)^{1/8} \exp\left[-\frac{1}{2}\left(\frac{V_0}{E_r}\right)^{1/2} k^2 x^2\right], \tag{16}$$

where k is the primary lattice wave vector. The amplitude of $W(x)$ rises with V_0 at each lattice site and, consequently, so does the amplitude of $g_2(r)$. Moreover, it has been found [62] that correlations arise from the interplay of quantum statistics, interactions, thermal, and quantum fluctuations, the last of which can be related to the higher harmonics in Eq. (15).

D. Test of $g_2(r)$ calculation by the WA

For the homogeneous Bose gas, we display in Fig. 4(c) the analytic result for $g_2(r)$ perturbative in $1/\gamma$ [55]

$$g_2^{(per)}(z, 1/\gamma) = 1 - \frac{\sin^2 z}{z^2} - \frac{4}{\gamma}\frac{\sin^2 z}{z^2} - \frac{2\pi}{\gamma}\frac{\partial}{\partial z}\frac{\sin^2 z}{z^2} + \frac{2}{\gamma}\frac{\partial}{\partial z}\left[\frac{\sin^2 z}{z^2}\int_{-1}^{1} dt\, \sin(zt)\ln\frac{1+t}{1-t}\right], \tag{17}$$

where $z = n\pi r$ and the one perturbative in γ,

$$g_2^{(per)}(r, \sqrt{\gamma}) = 1 - \sqrt{\gamma}[L_{-1}(2\sqrt{\gamma} n r) - I_1(2\sqrt{\gamma} n r)], \tag{18}$$

where, $L_{-1}(x)$ and $I_1(x)$ are the Struve and Bessel functions, respectively. Equation (17) is plotted with $\gamma = 10$ for the strongly interacting regime, whereas (18) is plotted with

$\gamma = 0.1$ for the weakly interacting regime. The goal is to check the WA $g_2(r)$ (e.g., for $\gamma = 2.000$) without an OL against analytic calculations, and one can see that the WA result lies largely intermediate between these analytic results. This shows again that WA is reliable in calculating these properties.

E. Origin of oscillations

Despite the fact that (17) displays weak oscillations, these are substantially enhanced in the WA $g_2(r)$ by the addition of an OL. The WA $g_2(r)$ for the Bose gas without an OL does not show any oscillations whatsoever (e.g., for $\gamma = 2.000$ and no OL in Fig. 4). It is known that strongly repulsive bosons in 1D without an OL arrange themselves in a periodic structure as if they were ordered inside an OL, but still the $g_2(r)$ reveals no spatial oscillations. The fact is that the OL introduces a different energy level structure that reshapes the wave function into a spatially oscillatory form.

Let us here only mention briefly the results of the appendixes and the reader is referred to the them for more information. In Appendix B, the SAPCF $h_2(r)$ [Eq. (11)] and the SA-OBDM $h_1(r)$ [Eq. (13)] are displayed in Figs. 7 and 8 (for the same systems of Figs. 3 and 4, respectively). The goal is to reveal the effects introduced into the correlations when instead of n^2 and n, the $g_2(r)$ and $g_1(r)$ are normalized by $\rho_c(r)$ and $\rho_{c,\frac{1}{2}}(r)$ [Eqs. (10) and (14)], respectively. [That is $g_1(r) \to h_1(r) = g_1(r)n/\rho_{c,\frac{1}{2}}(r)$ and $g_2(r) \to h_2(r) = g_2(r)n^2/\rho_c(r)$.] The result is that in general—for a shallow BCOL—$h_2(r)$ displays oscillations with a (much) smaller amplitude than $g_2(r)$. In fact, for a shallow BCOL, $h_2(r)$ is seen to approach the behavior of $g_2(r)$ for a homogeneous Bose gas. It can therefore be concluded that in this case the origin of the $g_2(r)$ oscillations is the oscillations in the spatial density whose structure is determined by the OL. In Appendix B, except for small oscillations, $h_1(r)$ shows generally the same qualitative behavior as $g_1(r)$.

In passing, it must be noted that the normalization by n^2 in $g_2(r)$, and by $\rho_c(r)$ in $h_2(r)$, just remains a matter of convenience regarding what purpose each one would achieve. For $g_2(r)$ this simply entails information about the density-density correlations and stronger signals than $h_2(r)$. For $g_1(r)$ and $h_1(r)$ it turns out that the normalization by n and $\rho_{c,\frac{1}{2}}(r)$, respectively, does not make much difference.

F. Interaction energy and local $g_2(0)$

According to Astrakharchik *et al.* [58], the total interaction energy $E_{\rm int}$ can be computed from $g_2(r)$ at $r = 0$ using

$$\frac{E_{\rm int}}{\langle N\rangle T_d} = \frac{1}{2} g_{1D} n g_2(0). \tag{19}$$

Now $E_{\rm int}$ goes to zero as γ is increased to large values beyond γ_c because $g_2(0) \to 0$. This can be seen in Fig. 4 for $\gamma > 6.250$ in all frames and is a stark indication to fermionization of the bosons [63] and demonstrates perfect antibunching [55]. In frame (c), fermionization is reached at $\gamma = 10$, whereas in frames (a) and (b) it requires $\gamma > 10$. Therefore, a larger V_0 aids the fermionization process of bosons since there is an enhanced effective interaction arising from the interplay between the BCOL and the repulsive forces that reduces the value of γ required for fermionization. The added secondary OL does not play a role in this regard.

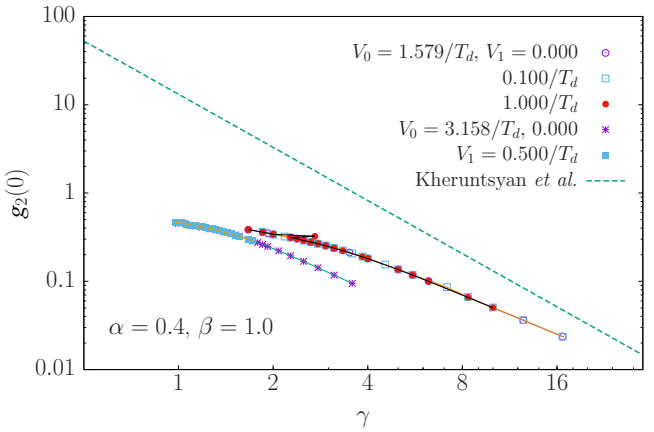

FIG. 5. Spatially averaged WA local pair correlation function $g_2(r = 0)$ [Eq. (8)] as a function of γ for the systems of Fig. 4 in comparison to $g^{(2)}(\gamma)$ of Kheruntsyan *et al.* [63] (dashed line) for the homogeneous Bose gas in the strongly interacting regime $\gamma > 1$. Here the QPOL is with $\alpha = 0.4$ and $\beta = 1.0$. The figure displays $g_2(0)$ for $V_0 = 1.579/T_d$ with $V_1 = 0$ (open circles), with $V_1 = 0.100/T_d$ (open squares), and with $V_1 = 1.000/T_d$ (solid circles). Then one has $V_0 = 3.158/T_d$ with $V_1 = 0.000$ (stars) and with $V_1 = 0.5/T_d$ (solid squares).

In Fig. 5, $g_2(0)$ is plotted as a function of γ for the two BCOLs with $V_0 = 1.579/T_d$ and $3.158/T_d$ and some values of V_1. For comparison, the analytical result for the homogeneous Bose gas of Ref. [63],

$$g^{(2)}(\gamma) = \frac{4}{3}\frac{\pi^2}{\gamma^2}\left[1 + \frac{t^2}{4\pi^2}\right], \tag{20}$$

with $t = T/T_d$ is displayed by the linear dashed line. It is immediately observed that, whereas, on the one hand, the introduction of an OL to a homogeneous Bose gas reduces $E_{\rm int}$ via a significant reduction of $g_2(0)$, the addition of a secondary weaker OL does not play much of a role in changing the behavior of $g_2(0)$ for the same V_0. The interaction in the system is therefore not influenced by a perturbation of the primary OL. The effect of γ on $g_1(r)$ shall be explored in a future publication in connection to the change of its behavior across the PT.

In Appendix D, $h_2(0)$ vs γ is displayed in Fig. 9 for the same systems of Fig. 5. Peculiarly, $h_2(0)$ shows qualitatively the same behavior of $g_2(0)$.

G. Matsubara Green's function

The MGF $G(p = 0,\tau)$ displays (1) the presence of a gas of particle-hole (p-h) pairs, revealing that the insulating state obtained following the PT is not inert similar to an MI [64] and (2) that the weight of p-h excitations declines with increasing γ. This is shown in Figs. 6(a) and 6(b), where $G(p = 0,\tau)$ decays at a faster rate with $|\tau|$ as γ is increased for any realization of the BCOL (we show here only two cases). In the limit when $\tau \to \pm\infty$, one can approximate $G(p = 0,\tau)$

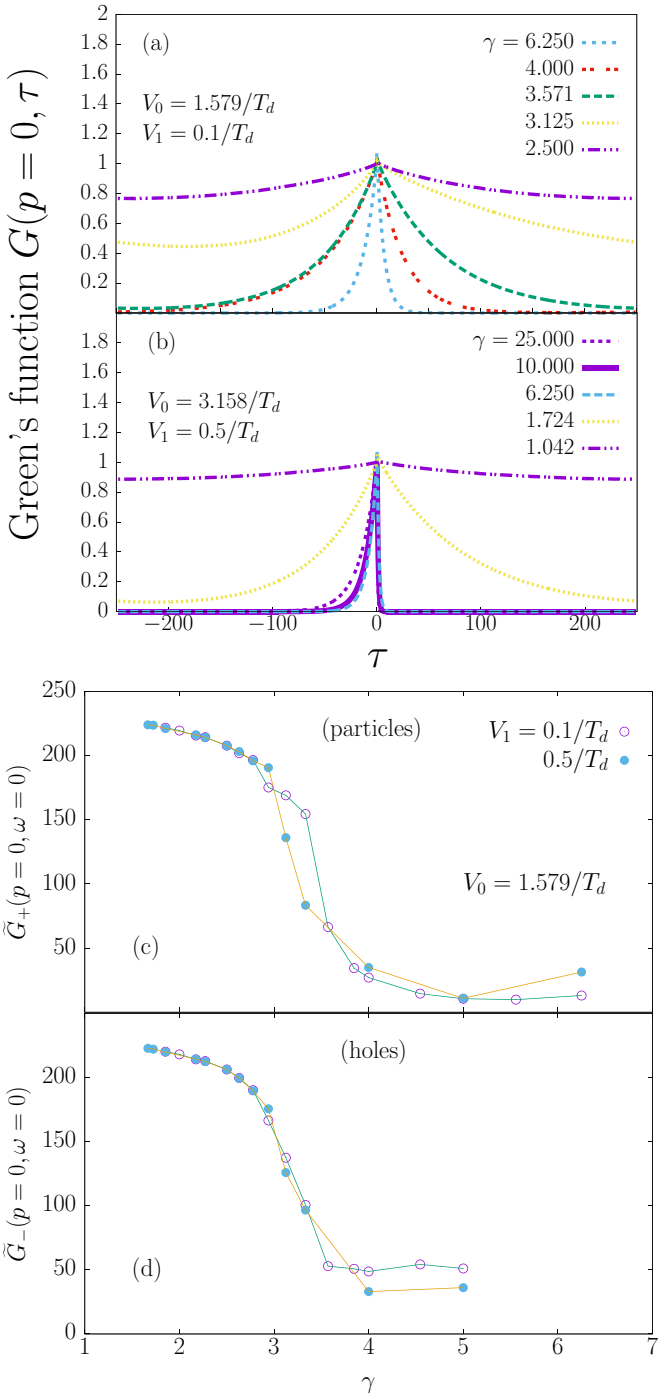

FIG. 6. Worm-algorithm Matsubara Green's function $G(p=0,\tau)$ and weights of particle and hole (p-h) excitations $\widetilde{G}_+(p=0,\omega=0)$ and $\widetilde{G}_-(p=0,\omega=0)$ [Eq. (24)], respectively, for the systems of Fig. 2. The top panels show G as a function of τ for some values of γ, and the bottom panels show $\widetilde{G}_\pm$ as a function of γ, all for different values of V_1. Panel (a) displays G for $V_0 = 1.579/T_d$ and $V_1 = 0.100/T_d$ with $\gamma = 6.250$ (dotted line), 4.000 (double-dotted line), 3.571 (dashed line), 3.125 (fine-dotted line), 2.500 (dash-triple-dotted line). Panel (b) is as in (a), but with $V_0 = 3.158/T_d$, $V_1 = 0.5/T_d$ and $\gamma = 25.000$ (dotted line), 10.000 (solid line), 6.250 (dashed line), 1.724 (fine-dotted line), 1.042 (dash-triple-dotted line). Frame (c) shows $\widetilde{G}_+$ for $V_0 = 1.579/T_d$ and $V_1 = 0.1/T_d$ (open circles), and $0.5/T_d$ (solid circles). Panel (d) is as in (c) with the same labels, but for $\widetilde{G}_-$. T and μ are in units of T_d and γ is unitless.

by [17]

$$G(p=0,\tau) \sim \begin{cases} e^{-E_P t}, & \tau \to +\infty \\ e^{+E_H t}, & \tau \to -\infty \end{cases} \tag{21}$$

where E_P and E_H are the single-particle and single-hole excitation energies, and $\tau = it$ is imaginary time. $G(p=0,\tau)$ reveals that for larger γ and $|\tau|$ higher values of E_P and E_H are required to induce p-h excitations. The lifetime of the p-h excitations $\sim \hbar/E_P$ or $\sim \hbar/E_H$, respectively, declines, therefore, with increasing γ as well. This demonstrates that because of the high repulsion the bosons become locked in their positions unable to move unless excited by a strong external perturbation. However, even after they are excited, they are deexcited after a short time as they return to the OL. Moreover, $G(p=0,\tau)$ is asymmetric about the origin $\tau = 0$, and particularly beyond the PT point γ_c, $G(p=0,\tau)$ displays higher probability for hole excitations than particles.

One can obtain a weight for the particle (hole) excitations from an integration of the area under $G(p=0,\tau)$ in the range $[0,\tau_{\max}]$ ($[-\tau_{\max},0]$), where $\tau_{\max} = 250$ is the maximum value of τ. In fact, an integration from $-\tau_{\max}$ to $+\tau_{\max}$ would be approximately equivalent to the Fourier transform of $G(p=0,\tau)$ at a frequency of excitation $\omega = 0$. We therefore consider for the present purpose

$$\widetilde{G}(p=0,\omega) \sim \int_{-\tau_{\max}}^{+\tau_{\max}} G(p=0,\tau) e^{-i\omega\tau} d\tau \tag{22}$$

and separate it into two terms:

$$\widetilde{G}(p=0,\omega) = \widetilde{G}_+(p=0,\omega) + \widetilde{G}_-(p=0,\omega), \tag{23}$$

where

$$\widetilde{G}_+(p=0,\omega) \sim \int_0^{\tau_{\max}} G(p=0,\tau) e^{-i\omega\tau} d\tau,$$
$$\widetilde{G}_-(p=0,\omega) \sim \int_{-\tau_{\max}}^{0} G(p=0,\tau) e^{-i\omega\tau} d\tau. \tag{24}$$

One can then define $\widetilde{G}_+(p=0,\omega=0)$ and $\widetilde{G}_-(p=0,\omega=0)$ as the weights of particle and hole excitations, respectively. $\omega = 0$ is chosen because there is no excitation agent in our simulations.

Figures 6(c) and 6(d) display $\widetilde{G}_+(0,0)$ and $\widetilde{G}_-(0,0)$ as functions of γ for $V_0 = 1.579/T_d$ and some values of V_1. Obviously, $\widetilde{G}_\pm$ decline with increasing γ and, moreover, both frames show an apparent change in the curvature of $\widetilde{G}_\pm$ close to the critical γ_c at which the PT occurs. Therefore, the change in the sign of $\partial^2\widetilde{G}_\pm(0,0)/\partial\gamma^2$ is a signal for the PT, and $\partial^2\widetilde{G}_\pm(0,0)/\partial\gamma^2 = 0$ near $\gamma = \gamma_c$.

IV. RATIONAL VS IRRATIONAL λ_1/λ_2

Whereas the ratio $\beta/\alpha = \lambda_1/\lambda_2$ is clearly rational for both pairs of $(\alpha,\beta) = (0.4,1.0)$ and $(0.4,1.39)$, it could be argued that had one used, for example, the irrational values $\widetilde{\alpha} = \sqrt{0.161} = 0.401\,248\ldots$, which is very close to 0.4, or $\widetilde{\beta} = \sqrt{1.9320} = 1.389\,964\ldots$, close to 1.39, the same results would be gotten as for $(0.4,1.39)$. Within this context, Table I lists δV [Eq. (2)] for various realizations of the BCOL at $(\widetilde{\alpha},\widetilde{\beta})$ and the rational approximation (α,β). It can be seen that the results of δV for (α,β) differ only slightly from that for $(\widetilde{\alpha},\widetilde{\beta})$

TABLE I. Standard deviation δV [Eq. (2)] for various realizations of the BCOL (1). From left to right, the table lists the primary-OL depth V_0, the secondary depth V_1, the standard deviation δV for $\alpha = 0.4$ and $\beta = 1.39$, and δV for $\widetilde{\alpha} = 0.401\,248\ldots$ and $\widetilde{\beta} = 1.389\,964\ldots$, respectively. V_0, V_1, δV are in units of T_d.

V_0 (T_d)	V_1 (T_d)	δV (α,β) (T_d)	δV $(\widetilde{\alpha},\widetilde{\beta})$ (T_d)
1.579	0.1	0.5594	0.5595
	0.5	0.5856	0.5857
	0.7	0.6107	0.6108
6.316	1.0	2.2609	2.2613
	3.0	2.4721	2.4726

by an order of magnitude $\lesssim 1\%$. In that sense, there should not be much difference in the results because of rational and irrational λ_1/λ_2.

V. CONCLUSION

In summary then, the properties of bosons in a shallow 1D BCOL, with a rational ratio λ_1/λ_2 of its wavelengths, have been examined by scanning the system along a range of the Lieb-Liniger parameter γ in the regime of the PT [5,7,13] described by the sine-Gordon model [6] at commensurate filling of the primary OL.

The chief result is that this PT in a primary OL of depth $V_0 \sim 1.5/T_d$ is robust against the perturbations by a secondary OL of depth $V_1 < V_0$. The critical interaction strength γ_c at which the PT occurs remains the same as for the periodic OL. The corresponding behavior of the SF fraction ρ_s/ρ vs γ reveals absolutely no response to changes in V_1; this is quite the same for other properties such as the correlation function $g_2(r)$ and the one-body density matrix $g_1(r)$. In contrast, changes in the latter observables arise with V_1 for larger values of $V_0 \sim 6/T_d$ at which the lattice-band structure of the primary OL begins to be influenced by the secondary OL. These results may turn out to be important in the research on hollow-core 1D fibers filled with ultracold atoms, where photons have been pinned by a shallow effective polaritonic potential just like atoms [9] and the quantum transport of strongly interacting photons [65].

However, for $V_0 \sim 1.5/T_d$ the properties are significantly affected by changes in γ. In this regard, $g_2(r)$ demonstrates an oscillatory structure whose amplitude rises with γ and V_0, manifesting an increase in the interplay between BCOL and interactions that yield the excitation of higher harmonics in the density operator. The origin of these oscillations lies chiefly in the primary OL. The latter changes are particularly significant beyond γ_c, reaching deep into the PT regime signaling the presence of a noninert Mott insulator in the form of a particle-hole gas of bosons. At very large γ beyond the critical γ_c, $g_2(0) \to 0$ signals fermionization and entrance to the Tonks-Girardeau regime. The fermionization process is aided by the primary OL and is unaffected by the secondary OL. Since $g_2(r)$ has been measured experimentally [18] over a broad range of the coupling strengths, our work should then motivate a future experimental measurement of $g_2(0)$ in a BCOL.

Although a division of $g_2(r)n^2$ and $g_1(r)n$ by the convoluted densities $\rho_c(r)$ and $\rho_{c,\frac{1}{2}}(r)$, respectively, yields qualitatively the same results as far as the sensitivity to changes in the BCOL is concerned, the response of $h_2(r) = g_2(r)n^2/\rho_c(r)$ to changes in V_0 and γ is, in general, significantly weakened. Hence, $g_2(r)$ is more adequate for obtaining stronger signals of changes. The $g_2(r)$ displays oscillations arising from oscillations in the spatial density that account for the same behavior in the density-density correlations.

The MGF $G(p = 0,\tau)$ displays a declining weight for the particle-hole excitations with rising γ attributed to an increased localization of the bosons. Moreover, it has been found that the system favors hole excitations at strong interactions, leading us to conclude that deep in the PT regime holes play a chief role in the response of $g_1(r)$ and $g_2(r)$ to γ. In addition, a change in the curvature of the Fourier transform of the MGF $G(p = 0,\omega = 0)$ as a function of γ for either particles or holes, is a signal for the PT.

An investigation that is very relevant to the present work is that by Gordillo *et al.* [12], who calculated the phase diagram of a continuous system of bosons in a BCOL. By keeping the interaction strength fixed, the SF fraction has been examined as a function of the secondary-OL depth for several values of the primary-OL depth within a range of amplitudes which is larger than ours. Among their findings, it has been demonstrated that changes in the secondary OL influence the properties and that an MI can be realized. In contrast, the present work conducts a similar investigation chiefly by varying the interaction strength in a *shallow* BCOL in a regime of interactions near the PT. Our studies therefore complement the work of Gordillo *et al.* and are further substantiated with the examination of the PT. Moreover, for a strong BCOL that we additionally considered, changes in the properties can be observed as one varies the intensity of the secondary OL bringing this is in line with the results of Gordillo *et al.* [12].

Finally, it must be emphasized that the WA code was able to reproduce the PT observed earlier by Haller *et al.* [5], Boéris *et al.* [7], and Astrakharchik *et al.* [13]. The investigation bearing similarities to ours by Boéris *et al.* [7] applied the WA to reproduce the PT, except that they only used a periodic OL with a different procedure than ours here. The current results are also in line with those of Edwards *et al.* [14], who demonstrated that the effects of weak perturbations to a primary 1D OL disappear as interactions get stronger and we *are* in the strongly interacting regime.

This work provides more clarification for the interplay between interactions and disorder for repulsive bosons in a quasidisordered OL as has been given earlier by Deissler *et al.* [30]. It is believed that this research will be an important contribution to the field of disordered bosons in 1D.

ACKNOWLEDGMENTS

Interesting and enlightening discussions with Sebastiano Pilati (ICTP, Trieste, Italy) are gratefully acknowledged, particulary for suggesting the topic on the pinning transition. Additional thanks go to Nikolay Prokofiev (UMASS, Amherst, MA, USA) for interesting discussions and for providing the worm-algorithm code. The author wishes to thank the Abdus-Salam International Center for Theoretical Physics (ICTP) in Trieste, Italy, and the Max Planck Institute for Physics of Complex Systems (MPIPKS) in Dresden, Germany, both for

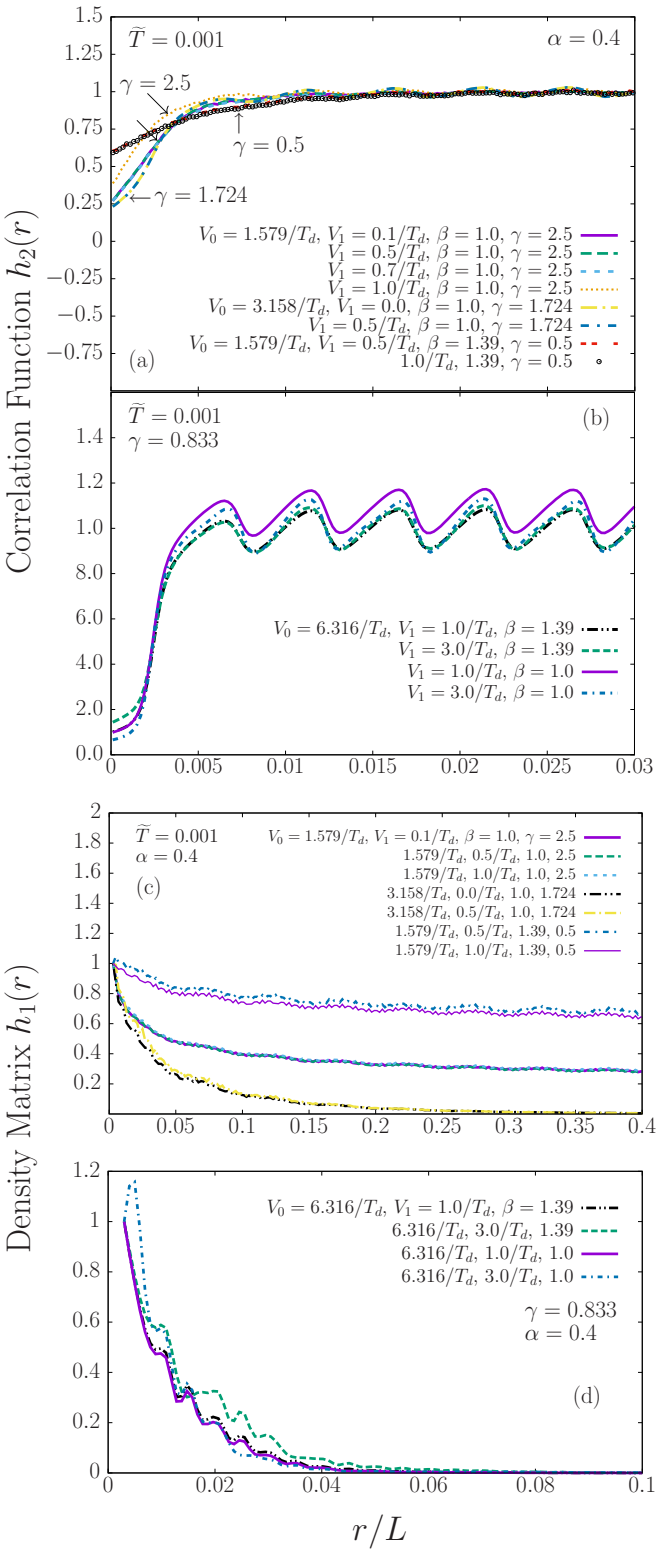

FIG. 7. As in Fig. 4, but for $h_2(r)$. (a) At $\gamma = 2.5$ and $V_0 = 1.579/T_d$ the figure displays the results for $V_1 = 0.1/T_d$, $\beta = 1.0$ (thick solid line); 0.5, 1.0 (thick-dashed line); 0.7, 1.0 (short-dashed line); 1.0, 1.0 (fine-dotted line). Then at $\gamma = 1.724$ and $V_0 = 3.158/T_d$ the results are shown for 0.0, 1.0 (long-dashed dotted line); 0.5, 1.0 (short-dashed dotted line). At $\gamma = 0.5$ and $V_0 = 1.579/T_d$ again the results are shown for $V_1 = 0.5/T_d$, $\beta = 1.39$ (double-dotted dotted line) and 1.0, 1.39 (open circles). Panel (b) is for $V_0 = 6.316/T_d$, $\gamma = 0.833$, and $V_1 = 1.0/T_d$, $\beta = 1.39$ (long-dashed double-dotted line); $3.0/T_d$: 1.39 (thick-dashed line); $1.0/T_d$, 1.0 (solid line); $3.0/T_d$, 1.0 (dash-dotted line). Panel (c) is for the same system in (a), but for $h_1(r)$ with $V_0 = 1.579/T_d$ and $V_1 = 0.1/T_d$, $\beta = 1.0$, $\gamma = 2.5$ (thick solid line); $0.5/T_d$, 1.0, 2.5 (long-dashed line); $1.0/T_d$, 1.0, 2.5 (short-dashed line). Then one has for $V_0 = 3.158/T_d$: $0.0/T_d$, 1.0, 1.724 (long-dashed double-dotted line): and $0.5/T_d$, 1.0, 1.724 (dash-dotted line). Next, one has for $V_0 = 1.579/T_d$: $0.5/T_d$, 1.39, 0.5 (short-dashed dotted line) and $1.0/T_d$, 1.39, 0.5 (thin solid line). Finally, panel (d) is for the same system in (b), but for $h_1(r)$: dashed double-dotted line: $V_1 = 1.0/T_d$, $\beta = 1.39$; dashed line: $3.0/T_d$, 1.39; thick solid line: $1.0/T_d$, 1.0; dash-dotted line: $3.0/T_d$, 1.0.

providing him access to their excellent computational cluster and for a hospitable stay during scientific visits in which this work was undertaken. We are grateful to G. Astrakharchik for providing us with their data displayed in Fig. 10. We thank William J. Mullin (UMASS, Amherst, MA, USA) for a critical reading of the manuscript. This work has been carried out during the sabbatical leave granted to the author Asaad R. Sakhel from Al-Balqa Applied University (BAU) during academic year 2014–2015.

APPENDIX A: WORM ALGORITHM

Specifically, a WA code is applied which has been written by Prokofev [56] originally for the simulation of 1D soft-core bosons without any trapping potential. A 3D version of this code, although for ^{4}He on graphite, has been described earlier [53]. The worm algorithm is a path-integral Monte Carlo technique whose configurational space is extended to include what one calls "worms." In this method, particles are described by Feynman's path-integral formulation as closed trajectories in space-time (diagonal configurations). Each trajectory is a closed chain of "beads" and each "bead" is a pair of positions of the same particle separated by a time τ along the imaginary-time axis in space-time. In a closed trajectory, the initial and final positions of the path are the same along the space axis. The method considers imaginary "time" as inverse temperature [66], i.e., $it/\hbar \leftrightarrow 1/(k_B T)$, where $\hbar$ is Planck's constant, k_B Boltzmann's constant, and T the temperature. The configuration of the system is updated by adding or removing open trajectories in space-time called "worms" (off-diagonal configurations) which are paths in space-time whose initial and final positions along the space axis are not the same. Therefore, the configuration of the system is divided into two sectors: the Z sector containing all the closed trajectories and the G sector containing one open trajectory, or worm. The code is designed to perform various updates on these worms via certain acceptance and rejection probabilities that are carefully weighted functions of, and including, the factors $\exp[-(\mathbf{r}_\ell - \mathbf{r}_{\ell-1})^2/(4\lambda\tau)]$ and $\exp[-\tau V(\mathbf{r}_\ell)]$. Here $\lambda = \hbar^2/(2m)$ with m the mass of a boson, $\tau \to 1/(M k_B T)$ is the imaginary-time step, with M the total number of beads constituting the particle's trajectory along the imaginary-time axis, $\mathbf{r}_\ell$ the position of the ℓth bead along the space axis, and $V(\mathbf{r}_\ell)$ the potential energy of bead ℓ. The above factors included in a worm-update probability are integrated along the time axis over the length of the trajectory being updated.

The beginning and end of the worm are termed MASHA and IRA, respectively, where MASHA precedes IRA along the imaginary-time axis. There are various types of updates: (1) INSERT or REMOVE, in which a worm is created and added to, or annihilated from, the configuration, respectively; (2) MOVE FORWARD or MOVE BACKWARD, which change the length of the worm in space-time along the imaginary-time axis; (3) RECONNECT, in which a worm is connected to a closed trajectory after opening it resulting in an exchange of particles (permutation); (4) CUT or GLUE, where a closed trajectory is cut open by removing, or an open trajectory is closed by adding, a short chain of beads, respectively. All these updates are described in more detail by the inventors of the technique [53].

APPENDIX B: PAIR CORRELATION FUNCTION FOR INHOMOGENEOUS 1D BOSE GASES

Figure 7 is as in Fig. 3, but for $h_2(r)$ given by Eq. (11). In panel (a) for low V_0, the amplitude of the spatial oscillations in $h_2(r)$ is substantially reduced compared to the corresponding $g_2(r)$. Although the $h_2(r)$ oscillations do not vanish completely, their amplitude does not change with V_1, which is the same for $g_2(r)$ in Fig. 3(a). Indeed, the $g_2(r)$ oscillations are caused by the oscillations in the convoluted density $\rho_c(r)$ [Eq. (10)], and a division of $g_2(r)n^2$ by $\rho_c(r)$ [to get $h_2(r)$] almost flattens $h_2(r)$ at larger r so that it oscillates close to 1. Any changes in the structure of $h_2(r)$ with V_1 are not detected. There is a weak role of the band structure of the BCOL and its disorder at low V_0.

As one increases V_0 in Fig. 7(b), the amplitude of oscillations in $h_2(r)$ rises similarly to $g_2(r)$. This time the normalization by $\rho_c(r)$ does not yield a significant suppression of the oscillations as it occurs in panel (a). Therefore, at larger V_0 there is an increased effect of the band structure of the BCOL and the disorder. Qualitatively, nevertheless, Fig. 7 shows the same effects as Fig. 3. That is to say that by either $g_2(r)$ or $h_2(r)$ one reaches qualitatively the same conclusions about the effect of V_1 on the strength of the correlations, namely that there is none at low V_0.

Figure 8 is the same as Fig. 4, but for $h_2(r)$. Here the effect of interactions γ at $r > 0.000\,25$ is substantially weakened by the division of $g_2(r)n^2$ by $\rho_c(r)$, but remains quite pronounced towards $r \to 0$. The effect of γ at larger r cannot therefore be significantly detected by $h_2(r)$ because the effect of interactions is absorbed by the normalization process. At $r = 0$, $h_2(r)$ displays a reduction with γ similar to Fig. 4 and shows the same decline as in Fig. 5 (see Sec. D below).

APPENDIX C: ONE-BODY DENSITY MATRIX FOR INHOMOGENEOUS 1D BOSE GASES

The SA-OBDM $h_1(r)$ [Eq. (13)] in panels (c) and (d) of Fig. 7 displays qualitatively the same behavior as the corresponding $g_1(r)$, except for small oscillations that are a result of normalizing by $\rho_{c,\frac{1}{2}}(r)$. In fact, at larger V_0, there is really not much difference in the qualitative structure of $h_1(r)$ and $g_1(r)$ in frames (d) of Figs. 7 and 3, respectively; both of them display small oscillations. Therefore, for larger V_0, $h_1(r)$ and $g_1(r)$ can both be applied on the same footage to draw conclusions about the SF depletion and role of the BCOL.

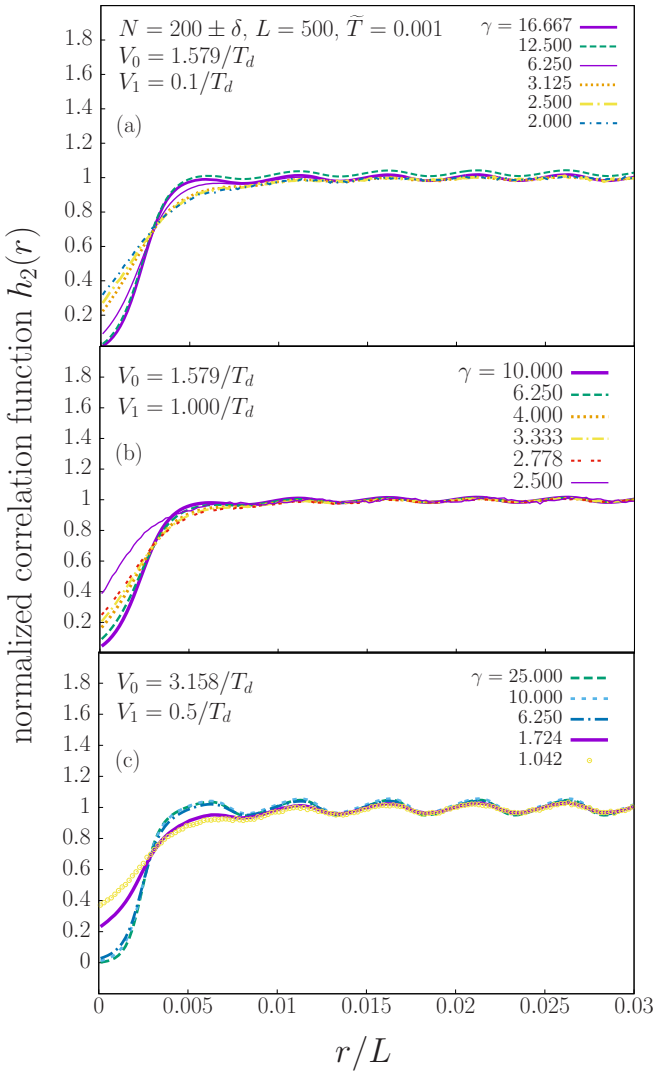

FIG. 8. As in Fig. 4, but for $h_2(r)$. (a) $V_0 = 1.579/T_d$, $V_1 = 0.1/T_d$, and $\gamma = 16.667$ (thick-solid line), 12.500 (dashed line), 6.250 (thin solid line), 3.125 (fine-dotted line), 2.500 (long-dashed dotted line), 2.000 (short-dashed dotted line). (b) $V_0 = 1.579/T_d$, $V_1 = 1.000/T_d$, and $\gamma = 10.000$ (solid line), 6.250 (dashed line), 4.000 (fine-dotted line), 3.333 (dash-dotted line), 2.778 (double-dotted line), 2.500 (thin solid line). (c) $V_0 = 3.158/T_d$, $V_1 = 0.5/T_d$, and $\gamma = 25.000$ (thick-dashed line), 10.000 (thin-dashed line), 6.250 (dash-dotted line), 1.724 (thick-solid line), 1.042 (circles).

APPENDIX D: LOCAL CORRELATION FUNCTION FOR INHOMOGENEOUS 1D BOSE GASES

The SAPCF at $r = 0$, i.e., $h_2(0)$, displays in Fig. 9 a drop with increasing γ and shows almost the same behavior as $g_2(0)$ in Fig. 5. Again, changes in V_1 for the same V_0 have no effect on $h_2(0)$.

APPENDIX E: TESTS OF THE WA CODE

In this section, the WA code [56] is tested on a uniform interacting Bose gas in the absence of any trapping potential.

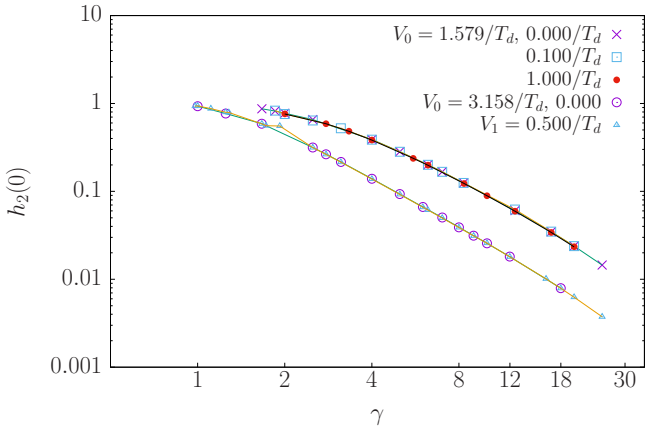

FIG. 9. As in Fig. 5, but for $h_2(0)$ with $V_0 = 1.579/T_d$ and $V_1 = 0$ (times), $0.1/T_d$ (open square), and $1.0/T_d$ (solid circles). Next data are for $V_0 = 3.158$ and $V_1 = 0$ (open circles) and $0.5/T_d$ (open triangles).

First, it is verified that the code produces the OBDM properly via a comparison with previous results. Second, it is confirmed that for suitably chosen parameters, the temperature of the simulations is low enough to obtain a significant SF fraction ρ_s/ρ. In this respect, WA results for ρ_s/ρ as a function of $\widetilde{T}$ were found to exactly match an analytical calculation.

1. One-body density matrix

The top panel of Fig. 10 displays the OBDM $g_1(r)$ as a function of nr at various $n|a_{1D}|$ obtained from WA simulations for three of the homogeneous Bose-gas cases already considered by Astrakharchik and Giorgini (AG) [58]. The values of $n|a_{1D}|$ range from the strongly to the weakly interacting regime as $n|a_{1D}|$ is increased. One can see that the agreement is excellent.

2. Superfluid fraction

The bottom panel of Fig. 10 displays a comparison between the SF fraction ρ_s/ρ obtained by WA and that by the equation

$$\rho_s/\rho = 1 - u\left|\frac{\theta_3''(0,e^{-2\pi u})}{\theta_3(0,e^{-2\pi u})}\right|, \tag{E1}$$

which is the same as Eq. (16) of Ref. [67], except that it is rescaled to our units. Here $u = 1/(2\widetilde{T}\langle N\rangle)$, with $\widetilde{T} = T/T_d$, $\langle N\rangle = 302$, and $L/a_{1D} = 50$. θ_3 is the Jacobi theta function of the third kind given by

$$\theta_3(z,q) = \sum_{n=-\infty}^{+\infty} q^{n^2}\exp(i2nz) \tag{E2}$$

and can be evaluated using Wolfram *Mathematica*. The system is a weakly interacting, dilute, and uniform 1D Bose gas whose

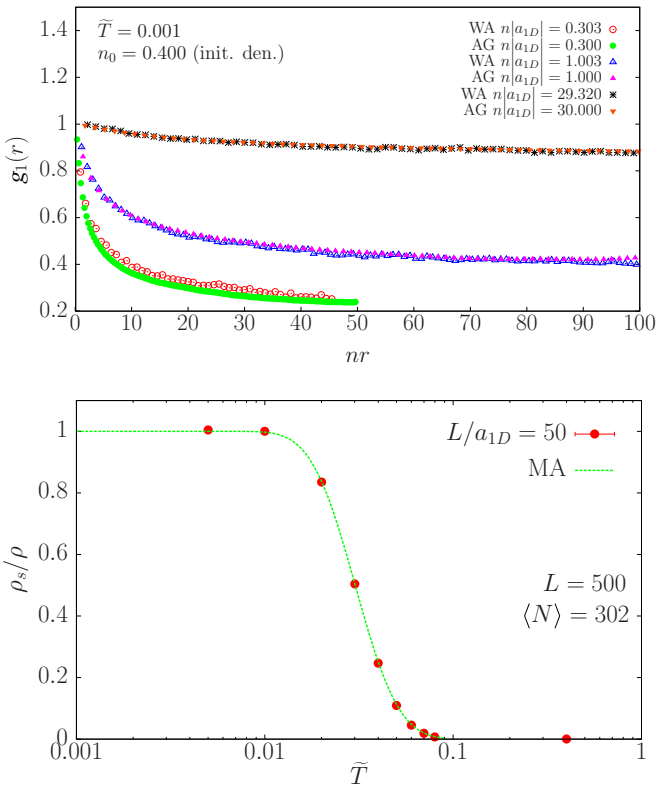

FIG. 10. (Top) Worm-algorithm first-order correlation function $g_1(r)$ (one-body density matrix) as a function of nr for several parameters $n|a_{1D}|$ compared to results from Astrakharchik and Giorgini (AG) [58] for values of $n|a_{1D}|$ which are almost identical to the WA ones. The system is a 1D homogeneous Bose gas at a temperature of $\widetilde{T} = 0.001$. Here n is the average linear density and a_{1D} the 1D scattering length. For the WA we have $n|a_{1D}| = 0.303$ (open circles), 1.003 (open up triangles), and 29.320 (stars), respectively. The corresponding data from AG are for almost the same $n|a_{1D}|$: 0.300 (solid circles), 1.000 (solid up triangles), and 30.000 (solid down triangles), respectively. (Bottom) Superfluid fraction ρ_s/ρ as a function of temperature $\widetilde{T}$. The system is again a 1D homogeneous gas of Bosons. The scattering length is $a_{1D}/L = 1/50$, the length of the system is $L/a_{1D} = 50$ and the thermodynamic average of the number of particles is $\langle N\rangle = 302$. The solid circles are the WA results, whereas the solid line is an analytical calculation using Eq. (E1) of Del Maestro and Affleck [67] with the same latter parameters. $\widetilde{T}$ is in units of the transition temperature T_d and the initial density of the WA simulation is $n_0 = 0.4$.

initial density was set to $n_0 = 0.2$ so that $T_d = 0.5027$. The WA results match exactly those of the analytical Eq. (E1), casting away all doubts about the accuracy of the WA code. Further, $\widetilde{T} = 0.001$ is low enough to allow a significant value for ρ_s/ρ. The reader must be alerted that the parameters used in this section and the previous one are only for the purpose of making the comparisons in Fig. 10. The rest of this paper uses the parameters of Sec. II F.

[1] P. Sengupta, M. Rigol, G. G. Batrouni, P. J. H. Denteneer, and R. T. Scalettar, Phys. Rev. Lett. **95**, 220402 (2005).

[2] Xia-Ji Liu, Peter D. Drummond, and Hui Hu, Phys. Rev. Lett. **94**, 136406 (2005).

[3] S. R. Clark and D. Jaksch, Phys. Rev. A **70**, 043612 (2004).
[4] S. Ramanan, T. Mishra, M. S. Luthra, R. V. Pai, and B. P. Das, Phys. Rev. A **79**, 013625 (2009).
[5] Elmar Haller, Russel Hart, Manfred J. Mark, Johann G. Danzl, Lukas Reichsöllner, Mattias Gustavsson, Marcello Dalmonte, Guido Pupillo, and Hanns-Christoph Nägerl, Nature (London) **466**, 597 (2010).
[6] H. P. Büchler, G. Blatter, and W. Zwerger, Phys. Rev. Lett. **90**, 130401 (2003).
[7] G. Boéris, L. Gori, M. D. Hoogerland, A. Kumar, E. Lucioni, L. Tanzi, M. Inguscio, T. Giamarchi, C. DErrico, G. Carleo, G. Modugno, and L. Sanchez-Palencia, Phys. Rev. A **93**, 011601(R) (2016).
[8] T. Giamarchi, *Quantum Physics in One Dimension*, 1st ed. (Oxford University Press, Oxford, UK, 2003).
[9] Ming-Xia Huo and Dimitris G. Angelakis, Phys. Rev. A **85**, 023821 (2012).
[10] L. Guidoni, C. Triché, P. Verkerk, and G. Grynberg, Phys. Rev. Lett. **79**, 3363 (1997).
[11] Nicolas Nessi and Anibal Iucci, Phys. Rev. A **84**, 063614 (2011).
[12] M. C. Gordillo, C. Carbonell-Coronado, and F. De Soto, Phys. Rev. A **91**, 043618 (2015).
[13] Grigory E. Astrakharchik, Konstantin V. Krutitsky, Maciej Lewenstein, and Ferran Mazzanti, Phys. Rev. A **93**, 021605(R) (2016).
[14] E. E. Edwards, M. Beeler, Tao Hong, and S. L. Rolston, Phys. Rev. Lett. **101**, 260402 (2008).
[15] D. J. Boers, B. Goedeke, D. Hinrichs, and M. Holthaus, Phys. Rev. A **75**, 063404 (2007).
[16] C. J. Pethick and H. Smith, *Bose-Einstein Condensation in Dilute Gases*, 1st ed. (Cambridge University Press, Cambridge, UK, 2002).
[17] Maciej Lewenstein, Anna Sanpera, and Verónica Ahufinger, *Ultracold Atoms in Optical Lattices: Simulating Quantum Many-Body Systems* (Oxford University Press, Oxford, UK, 2012).
[18] Toshiya Kinoshita, Trevor Wenger, and David S. Weiss, Phys. Rev. Lett. **95**, 190406 (2005).
[19] B. Deissler, E. Lucioni, M. Modugno, G. Roati, L. Tanzi, M. Zaccanti, M. Inguscio, and G. Modugno, New J. Phys. **13**, 023020 (2011).
[20] G. Roux, T. Barthel, I. P. McCulloch, C. Kollath, U. Schollwöck, and T. Giamarchi, Phys. Rev. A **78**, 023628 (2008).
[21] T. Roscilde, Phys. Rev. A **77**, 063605 (2008).
[22] M. Larcher, M. Modugno, and F. Dalfovo, Phys. Rev. A **83**, 013624 (2011).
[23] M. Modugno, New J. Phys. **11**, 033023 (2009).
[24] R. Roth and K. Burnett, Phys. Rev. A **67**, 031602(R) (2003).
[25] S. Pilati, S. Giorgini, M. Modugno, and N. Prokof'ev, New J. Phys. **12**, 073003 (2010).
[26] I. L. Aleiner, B. L. Altshuler, and G. V. Shlyapnikov, Nat. Phys. **6**, 900 (2010).
[27] P. Lugan, A. Aspect, L. Sanchez-Palencia, D. Delande, B. Grémaud, C. A. Müller, and C. Miniatura, Phys. Rev. A **80**, 023605 (2009).
[28] M. White, M. Pasienski, D. McKay, S. Q. Zhou, D. Ceperley, and B. DeMarco, Phys. Rev. Lett. **102**, 055301 (2009).
[29] L. Fallani, J. E. Lye, V. Guarrera, C. Fort, and M. Inguscio, Phys. Rev. Lett. **98**, 130404 (2007).
[30] B. Deissler, M. Zaccanti, G. Roati, C. DÉrrico, M. Fattori, M. Modugno, G. Modugno, and M. Inguscio, Nat. Phys. **6**, 354 (2010).
[31] G. Roati, C. DÉrrico, L. Fallani, M. Fattori, C. Fort, M. Zaccanti, G. Modugno, M. Modugno, and M. Inguscio, Nature (London) **453**, 895 (2008).
[32] J. Billy, V. Josse, Z. Zuo, A. Bernard, B. Hambrecht, P. Lugan, D. Clément, L. Sanchez-Palencia, P. Bouyer, and A. Aspect, Nature (London) **453**, 891 (2008).
[33] Y. P. Chen, J. Hitchcock, D. Dries, M. Junker, C. Welford, and R. G. Hulet, Phys. Rev. A **77**, 033632 (2008).
[34] M. P. A. Fisher, P. B. Weichman, G. Grinstein, and D. S. Fisher, Phys. Rev. B **40**, 546 (1989).
[35] J. Bossy, J. V. Pearce, H. Schober, and H. R. Glyde, Phys. Rev. B **78**, 224507 (2008).
[36] S. Palpacelli and S. Succi, Phys. Rev. E **77**, 066708 (2008).
[37] D. Clément, A. F. Varón, J. A. Retter, L. Sanchez-Palencia, A. Aspect, and P. Bouyer, New J. Phys. **8**, 165 (2006).
[38] X. Deng, R. Citro, E. Orignac, A. Minguzzi, and L. Santos, Phys. Rev. B **87**, 195101 (2013).
[39] L. Pollet, N. V. Prokof'ev, and B. V. Svistunov, Phys. Rev. B **87**, 144203 (2013).
[40] Z. Ristivojevic, A. Petković, P. Le Doussal, and T. Giamarchi, Phys. Rev. Lett. **109**, 026402 (2012).
[41] S. Iyer, D. Pekker, and G. Rafael, Phys. Rev. B **88**, 220501(R) (2013).
[42] D. M. Basko and F. W. J. Hekking, Phys. Rev. B **88**, 094507 (2013).
[43] T. Schulte, S. Drenkelforth, J. Kruse, W. Ertmer, J. Arlt, K. Sacha, J. Zakrzewski, and M. Lewenstein, Phys. Rev. Lett. **95**, 170411 (2005).
[44] T. Paul, P. Schlagheck, P. Leboeuf, and N. Pavloff, Phys. Rev. Lett. **98**, 210602 (2007).
[45] L. Sanchez-Palencia, D. Clément, P. Lugan, P. Bouyer, G. V. Shlyapnikov, and A. Aspect, Phys. Rev. Lett. **98**, 210401 (2007).
[46] P. Lugan, D. Clément, P. Bouyer, A. Aspect, and L. Sanchez-Palencia, Phys. Rev. Lett. **99**, 180402 (2007).
[47] T. Paul, M. Albert, P. Schlagheck, P. Leboeuf, and N. Pavloff, Phys. Rev. A **80**, 033615 (2009).
[48] J. Radić, V. Bačić, D. Jukić, M. Segev, and H. Buljan, Phys. Rev. A **81**, 063639 (2010).
[49] J. C. C. Cestari, A. Foerster, and M. A. Gusmão, Phys. Rev. A **82**, 063634 (2010).
[50] S. Iyer, D. Pekker, and G. Refael, Phys. Rev. B **85**, 094202 (2012).
[51] C. Aulbach, A. Wobst, G. L. Ingold, P. Hänggi, and I. Varga, New J. Phys. **6**, 70 (2004).
[52] X. Deng and L. Santos, Phys. Rev. A **89**, 033632 (2014).
[53] M. Boninsegni, N. V. Prokof'ev, and B. V. Svistunov, Phys. Rev. E **74**, 036701 (2006).
[54] E. H. Lieb and W. Liniger, Phys. Rev. **130**, 1605 (1963).
[55] A. G. Sykes, D. M. Gangardt, M. J. Davis, K. Viering, M. G. Raizen, and K. V. Kheruntsyan, Phys. Rev. Lett. **100**, 160406 (2008).
[56] Nikolay Prokof'ev (private communication).
[57] R. P. Feynman, *Statistical Mechanics* (Westview Press, Boulder, CO, 1998).
[58] G. E. Astrakharchik, J. Boronat, J. Casulleras, and S. Giorgini, Phys. Rev. Lett. **95**, 190407 (2005).
[59] See Eq. (13.37) on p. 349 in Ref. [16].

[60] The spatially averaged normalized second-order correlation function is given by Naraschewski *et al.* [61] by their Eq. (2.21) and is effectively the same as ours:

$$g^{(2)}(r) = \frac{\int d\mathbf{R} G^{(2)}\left(\mathbf{R} - \frac{\mathbf{r}}{2}, \mathbf{R} + \frac{\mathbf{r}}{2}\right)}{\int d\mathbf{R} G^{(1)}\left(\mathbf{R} - \frac{\mathbf{r}}{2}, \mathbf{R} - \frac{\mathbf{r}}{2}\right) G^{(1)}\left(\mathbf{R} + \frac{\mathbf{r}}{2}, \mathbf{R} + \frac{\mathbf{r}}{2}\right)},$$

where

$$G^{(1)}(\mathbf{r}, \mathbf{r}') = \langle \hat{\Psi}^{\dagger}(\mathbf{r}) \hat{\Psi}(\mathbf{r}') \rangle$$

and

$$G^{(2)}(\mathbf{r}, \mathbf{r}') = \langle \hat{\Psi}^{\dagger}(\mathbf{r}) \hat{\Psi}^{\dagger}(\mathbf{r}') \hat{\Psi}(\mathbf{r}') \hat{\Psi}(\mathbf{r}) \rangle.$$

If we shift the coordinates $\mathbf{R} - \mathbf{r}/2$ and $\mathbf{R} + \mathbf{r}/2$ by adding $\mathbf{r}/2$, this becomes essentially equivalent to our expression Eq. (14), except that we consider a 1D system and the integration is from $x = 0$ to L.

[61] M. Naraschewski and R. J. Glauber, Phys. Rev. A **59**, 4595 (1999).

[62] A. Y. Cherny and J. Brand, Phys. Rev. A **79**, 043607 (2009).

[63] K. V. Kheruntsyan, D. M. Gangardt, P. D. Drummond, and G. V. Shlyapnikov, Phys. Rev. Lett. **91**, 040403 (2003).

[64] S. S. Natu and E. J. Mueller, Phys. Rev. A **87**, 063616 (2013).

[65] M. Hafezi, D. E. Chang, V. Gritsev, E. Demler, and M. D. Lukin, Phys. Rev. A **85**, 013822 (2012).

[66] G. D. Mahan, *Many-Particle Physics* (Plenum Press, New York, 1990).

[67] A. D. Maestro and I. Affleck, Phys. Rev. B **82**, 060515(R) (2010).